EFFICIENT STRAYEGY SELECTION OF PERMANENT AND DISTRIBUTED SCATTERERS IN NON-URBAN AREAS

Mohamed Fekir(1), Faiza Hocine(1), Afifa Haddoud(1), Aichouche Belhadj-aissa(1)

(1) University of Sciences and Technology Houari Boumediene (USTHB)
Laboratory of Image Processing and Radiation, Faculty of Electronics and Computer Science.
BP. 32, El Alia, Bab Ezzouar 16011, Algiers, Algeria
fekirm@gmail.com, h.belhadj@lycos.com

ABSTRACT

The differential interferometry PSI is based on the identification of targets exhibiting good phase stability PS. These targets are available in urban areas, but less available in non-urban areas. For this purpose, the statistically homogeneous pixels DS, permit to this technique to be extended for the non-urban areas. Knowing that homogeneous areas are favourable for a development of the speckle noise, an adaptive filtering is applied to these areas without compromising the phase stability of PS. In this context, we propose in this paper a PS and DS selection strategy based on two steps: first, the PS are selected and isolated using coherence maps, which will allow us to exclude theme from filtering operation. In the second step, the DS selection is processed.
This approach has been tested on SAR images acquired by sensors ERS1/2 corresponding to the area of Haoud el Barkaoui, Ouargla in Algeria.

Keywords-- PSI; Permanent scatterers ; Distributed scatterers ; coherence Matrix; phase triangulation

1. INTRODUCTION

The detection of ground motion using differential interferometry SAR (Synthetic Aperture Radar) has given excellent results in many application domains.
Differential SAR interferometry (DInSAR) uses the phase difference (interferogram) between two SAR images of the same scene, acquired in different dates. This phase difference mainly contains two useful informations: information about the terrain and another on the ground displacement occurred between the dates of acquisition. In its basic principle, the DInSAR measures the deformation between two acquisitions by removing topographic information; it is the single pass DInSAR. This configuration does not allow access to the shape and the deformation rate in the study time interval. The answer to this preoccupation is the use of time series SAR images, which is possible with the development of SAR sensors and the availability of a large archive of SAR images. However, the major difficulty in the treatment and exploitation of these acquisitions is the diversity of spatial and temporal baselines used to build all the differential interferograms with important spatial and temporal decorrelation, added to this, the significant errors phases introduced by atmospheric layers [1].
Since the early 2000s, a new dimension has been given to this technique with a dual purpose of being able to use all available data and try to overcome the most of these limitations (décorélations). Among the proposed approaches, we include the PSI (permanent scatterers interferometry) approach [2-4]. This approach aims to identify pixels with a single dominant response in the cell resolution and a good phase stability PS (Permanent Scatterer), these pixels are less affected by the correlation and allow us to use the associated interferometric phases to infer the time series of the deformation. The PSI concept has been successfully applied in urban applications. But its effectiveness is defective in non-urban areas (scarcity of PS (s)). To this end, the same initiators of this concept have proposed an alternative approach to strengthen the process of PSI in non-urban areas [5]. This approach aims to exploit the statistically homogeneous pixels, so-called DS (Distributed scatterers). Those statistically homogeneous areas are favorable to the development of speckle noise. Once selected, the DS require an adaptive filtering without compromising the stability Phase of the PS(s).
In this context, the paper we propose focuses on a selection strategy of PS and DS. This strategy selection is based on two steps; first, the PS are selected and isolated, which will allow us to exclude theme from filtering operation. In the second step, the DS are selected, filtered and optimized to finally select the select those who will joining the PS to form a dense sparse grid.

2. PROPOSED APPROACH

The selection strategy we propose is represented by the flowchart Fig. 1. The PS selection is carried out using the coherence maps generated from interferometric pairs with small baselines [7-9]. The DS selection is carried out using amplitude images.

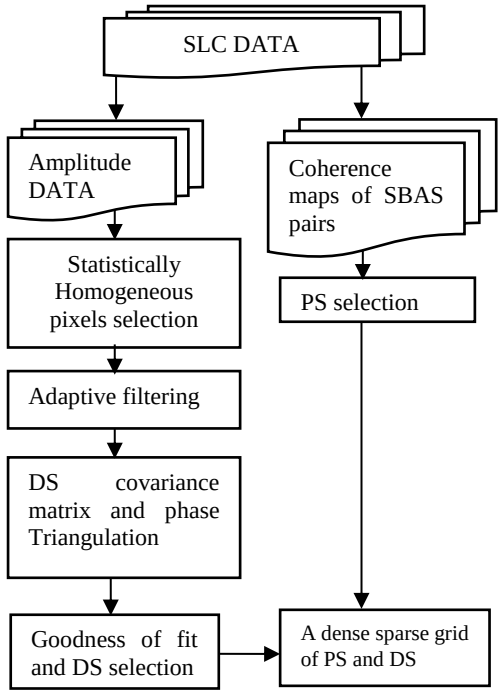

Figure 1. Strategy selection flowcharts

2.1 PS Selection

The PS selection can be carried out using the amplitude images, or coherence maps. The amplitude dispersion index is a good criterion selection [3], however, this criterion requires a number of images greater than 30, which is not the case for our study area. In this context, we used coherence maps [6].

The coherence maps are generated from pairs having small baselines. The interconnection of image pairs is illustrated in Fig. 2. Some subsets are eliminated because they have large baselines. We also note that the images acquired by the ERS-2 sensor beyond the year 2003, were excluded because of their poor quality.

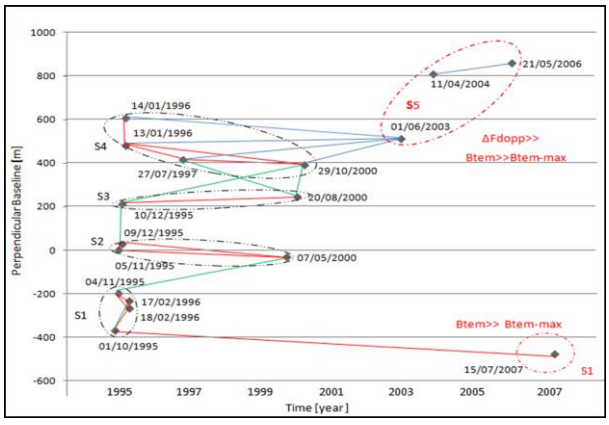

Figure 2. Pair images interconnections in spatial-temporal plane

These targets are selected from statistical descriptors computed for each coherence map. For this purpose, the spatial threshold (T_s) is calculated and is based on the distribution of the coherence values around the mean Eq. 1.

$$T_{si} = \sqrt{\mu_i(1-\sigma_i)} \quad (1)$$

Where, μ_i is the average local map coherence i and σ_i is its standard deviation. The coherent targets are selected If there average temporal coherence is greater than the threshold given by Eq. 2.

$$T_{th} = \sqrt[k]{\prod_{i=1}^{k} T_{si}} \quad (2)$$

2.2. DS Selection

The distributed scatterers DS(s) are defined as a groups of neighboring pixels belonging to areas of moderate coherence in some interferometric pairs of the available data-set, and they share similar reflectivity values, as they belong to the same object. These targets usually correspond to debris areas, non-cultivated land with short vegetation or desert areas [5].

Two image pixels P1 and P2 will be defined as statistically homogenous if the null hypothesis that the two image vectors d(P1) and d(P2) of respectively pixels P1 and P2 are drawn from the same probability distribution function (p.d.f.). To select this homogeneous statistical population, for each image-pixel, statistical tests are applied to all pixels within a certain estimation window centered on the pixel under analysis.

The KS (Kolmogorov Smirnov) test is one of some nonparametric tests that can achieve the comparison between the two image vectors. It is based on the maximum difference between the distribution of distribution functions Fig .3, the maximum difference is given by Eq .3.

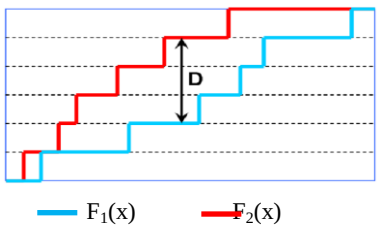

Figure 3. The maximum difference illustration

$$D = max_x |F_1(x) - F_2(x)| \quad (3)$$

The N values of the image vector can be converted to an unbiased estimator $S_N(X)$of the law of probability of the cumulative distribution function, whose expression is given by Eq. 4:

$$S_N(X) = \begin{cases} 0, si\ \ X < x_1 \\ \frac{k}{N}, si\ \ x_k \le X < x_{k+1} \\ 1, si\ X \ge x_N \end{cases} \quad (4)$$

Where, x_k is k[th] element of image vector. To assess if the two pixels P1 and P2 are statistically homogeneous (similarity between distribution functions), the KS test measures the absolute difference D_N between the cumulative probability distributions functions S_N^{P1} and S_N^{P2} Eq. 5

$$D_N = \sqrt{N/2}\, sup_{x \in R} |S_N^{P1}(x) - S_N^{P2}(x)| \quad (5)$$

Which can be approximated by the KS distribution whose cumulative distribution function H (t) is given by Eq. 6.

$$P(D_N \le t) = H(t) = 1 - 2\sum_{n=1}^{\infty}(-1)^{n-1} e^{-2n^2t^2} \quad (6)$$

$H(t)$ does not depend on the cumulative distribution function of specific data.

The KS test considers the two vectors to be compared are statistically homogeneous if $D_N \le c$, the threshold c depends on significance level set α, where α is a threshold that depends on the size of the vector (number of images), the values of α are defined for each N images.

The central pixel of estimation window is compared to adjacent pixels. Finally, two statistically homogeneous pixels are classified as follows;

- If they do not belong to any class (group), a new class is created containing the two pixels
- If one of the two pixels already belongs to a class, the second will join it in the same class
- If each of the pixels is belonging to a different class, then we merge the two classes.

Moreover, to ensure proper distribution of the classes throughout the space with and optimization of their number, we proceeded to the reduction of the number of groups taking as a threshold the number of pixels in the window estimation. In our case, we have used a window of 9x9. These groups of statistically homogeneous pixels are contiguous regions of pixels, than we cannot use the design to build a network of arcs on which is based the mathematical model for estimating of the different components of the differential phase. For this reason, a full major step processing, is to looking for in each DS, an optimal phase vector, then correct the phases of each element of the DS with respect to this vector and then select the most consistent of them to be taken as PS.

Under the assumption of Gaussian dispersion based on the central limit theorem, the data vector can be described by a probability distribution function of multidimensional complex Gaussian, with zero mean. Thus, for a full statistical characterization of a DS, the covariance matrix Eq. 7 is calculated for each group of DS.

$$C(p)_{(N,N)} = E[d\ d^T] \approx \frac{1}{|\Omega|}\sum_{P \in \Omega} d(p) d(p)^H \quad (7)$$

Where, d(p) is the image vector of pixel P, H is the Hermitian operator, Ω is the number of elements in the DS region and N the number of images.

The diagonal elements of the covariance matrix are the values of the intensities, while the values of the off-diagonal elements correspond to the filtered interferometric phases. By normalizing the amplitude data such that $E[|d_i|^2] = 1$ for all i, we can deduce the complex coherence matrix Eq. 8 , also, the phase values of the matrix correspond to the filtered interferometric phase values, noted(ϕ_{kj}).

$$\hat{\Gamma} = \{\gamma_{kj}.\, e^{i\phi_{kj}}\} \quad (8)$$

The quality of a DS can be done from the coherence matrix. If we represent the modulus of the matrix consistency, more the values are high in the elements of off diagonal, more the elements forming the DS region are consistent.

The idea is to find an optimal vector of N phase values $v = [v_1, v_2, \dots, v_N]$, corresponding to those of off-diagonal elements of the matrix $\hat{\Gamma}$. The coherence matrix of pixel P could be formulated by Eq. 9.

$$\Gamma(P) = \Theta \Upsilon \Theta^H \quad (9)$$

Where, Υ is a symmetric matrix of *NxN* elements, with actual values correspond to the coherence values of all *N* interferograms and Θ is a *NxN* diagonal matrix $\Theta = \text{diag}\{\exp(j\theta)\}$, it contains the true phase values of the pixel P.

Assuming that all the pixels belonging to Ω are described by the same set of θ phase values, the probability distribution functions of the statistically homogeneous pixels can then be expressed by Eq. 10.

$$p(d_\Omega|\theta) \propto \prod_{P\, \epsilon\, \Omega} exp(-d_P^H \Theta \Upsilon^{-1} \Theta^H d_P) \quad (10)$$

$$= \exp[-trace(\Theta \Upsilon^{-1} \Theta^H \hat{\Gamma})]$$

The maximum likelihood (ML) of θ is obtained by maximizing the probability distribution function or by minimizing the absolute value. Since only the phase differences appear in $\widehat{\Gamma}$, the phase values can be estimated to an arbitrary additive constant. Without loss of generality, we can define the interferometric phase of

the first image to zero.
The best estimate of the (N – 1) phase values, $\lambda = [0, \theta_2. . ., \theta_N]^T$ is given by Eq. 11.

$$\hat{\lambda} = argmax\{ exp[-trace(\Phi \Upsilon^{-1} \Phi^H \hat{\Gamma})] \} \quad (11)$$

$$= argmax\{ exp[-\Lambda^H (\Upsilon^{-1} \circ \hat{\Gamma}) \Lambda] \}$$

$$= argmax\{ \Lambda^H (\Upsilon^{-1} \circ \hat{\Gamma}) \Lambda \}$$

Where, Φ is $N \times N$ diagonal matrix, Φ =diag {exp (i λ)}, Λ is N dimension vector with Λ = exp (i λ) and $\circ$ is the Hadamard product.
The algorithm requires the nonlinear minimization of a function, which implies the use of iterative methods. One possible solution is the Quasi-Newton algorithm. In our case we used the BFGS (Broyden Fletcher Goldfarb Shannon) algorithm to achieve the estimation of optimal phase vector.
To achieve the selection of the most consistence pixels from each DS, a goodness of fit is calculated by Eq. 12.

$$\gamma_{PTA} = \frac{2}{N^2 - N} Re \sum_{n=1}^{N} \sum_{k=n+1}^{N} e^{i\phi_{nk}} \; e^{-i(\theta_n - \theta_k)} \quad (12)$$

This goodness of fit is used as threshold to select the DS.

3. RESULTS AND INTERPRETAION

This approach has been tested on SAR images acquired by sensors ERS1/2 corresponding to the area of Haoud el Barkaoui, Ouargla in Algeria Tab. 1. This region is characterised by subsidence due to the upwelling. Also, we note that some images acquired by the ERS-2 sensor beyond the year 2003 were discarded because of their poor quality.

Table 1. SAR images used in the application

Mission	Orbits	Acquisition Date	Normal baseline (m)	Temp baseline (days)	ΔF Doppler (Hz)
ERS2	2338	01/10/1995	-370	35	0
ERS1	22512	04/111995	-199	1	-229
ERS2	2838	05/11/1995	0	0	0
ERS1	23013	09/12/1995	27	34	-229
ERS2	3340	10/12/1995	211	35	0
ERS1	23514	13/01/1996	480	69	-229
ERS2	3841	14 /01/1996	606	70	0
ERS1	24015	17/02/1996	-234	104	-229
ERS2	4342	18/02/1996	-268	105	0
ERS2	11857	27/07/1997	415	630	0
ERS2	26386	07/05/2000	-32	1645	-191
ERS2	27889	20/08/2000	244	1750	330
ERS2	28981	29/10/2000	391	1820	105

The sparse grid of strong coherent pixels PS selected by coherence maps is illustrated in Fig. 4.

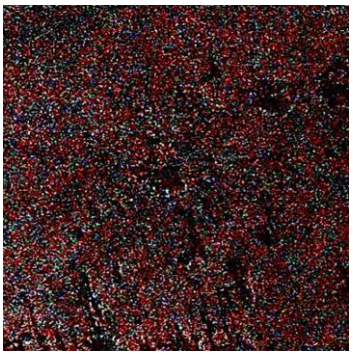

Figure 4. Grid of PS

The statistically homogeneous pixels classes (groups) selected by KS test are illustrated in Fig. 5. We note that some groups smaller than estimation windows size should be eliminated and the resultant groups should despeckled (filtered).

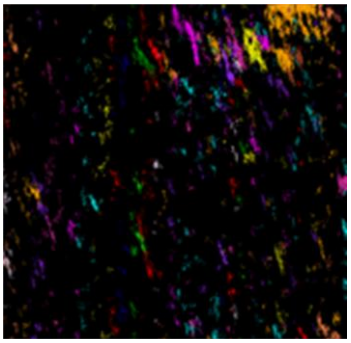

Figure 5. Different statistically homogeneous pixels groups selected by KS test

Once the DS filtered, we calculate the covariance matrix for each DS to have its statistical characterization. We give in Fig. 6, three examples of covariance matrices of three different DS.

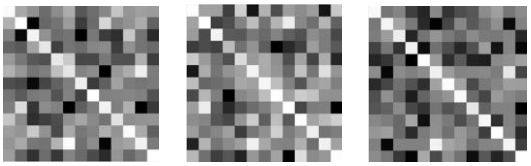

Figure 6. Three examples of DS covariance matrix

The coherence matrices are deduced from covariance matrices by normalizing the diagonal elements. The off diagonal elements represent also the filtred interferometric phases. Moreover, an optimal phase vector is estimated for each DS by BFGS algorithm. Then, the DS are selected by applying a goodness of fit. The fusion of PS and DS in same sparse grid is illustrated in Fig. 7.

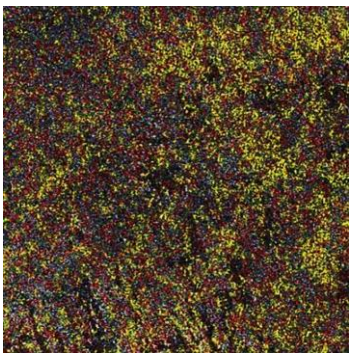

Figure 7. Grid of PS and DS

The Delaunay triangulation makes interconnections (arcs) between selected pixels in sparse grid. On each arc, a difference of differential phase is calculated to remove the atmospheric contribution supposed spatially correlated in a certain length. If the grid is less dense, the arcs are longer and the atmospheric is not totally removed.

The Delaunay triangulation of PS grid is illustrated in fig. 8, we notice some longer arcs in certain regions framed in red, this, will not allow a total subtraction of the atmospheric contribution, which will influence the estimated results.

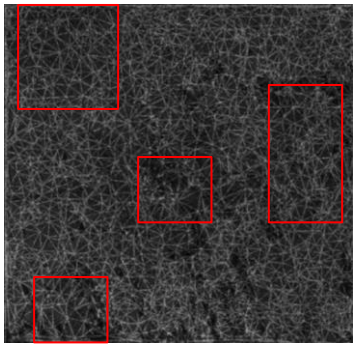

Figure 8. Delaunay triangulation of PS grid

By against, The Delaunay triangulation of PS and DS grid is done in Fig. 9, we notice some improvement on the lengths of the arcs in a certain regions.

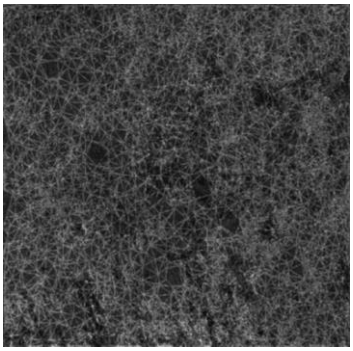

Figure 9. Delaunay triangulation of PS and DS grid

4. CONCLUSION

This paper, proposes a strategy selection of both strong coherent pixels in resolution cell PS and the distributed scatterers DS. The selection of PS is fed through the coherence maps generated from pair images characterised by small baselines. These very strong pixels have very high phase stability, so it should be forewarned from the average filtering of statistically homogeneous pixels. The results show enhancement in the grid density, which allows a good estimation of soil subsidence. The main drawback of this strategy selection is the computational costs and large memory space.

5. REFERENCES

1. Zebker, H. A., Villasenor, J., (1992). Decorrelation in Interferometric Radar Echoes, IEEE Trans. Geosci. Remote Sens., vol.30, No.5, p.950–959.
2. Ferretti, A., Prati, C. et Rocca, F. (2000). Nonlinear subsidence rate estimation using permanent scatterers in differential SAR interferometry. IEEE Trans. Geosci. Remote Sensing, Vol. 38, N0. 5.
3. Ferretti, A., Prati, C. et Rocca, F. (2001) Permanent Scatterers InSAR interferometry. IEEE Trans. Geosci. Remote Sensing, Vol 39, N. 1.
4. Kampes, B. M., et Hanssen, R. (2004). Ambiguity Resolution for Permanent Scatterer Interferometry. IEEE Trans. Geoscience. Remote Sensing, Vol. 42, N0. 11, p.
5. Ferretti, A., Fumagalli, A. et Novali,F. (2011). A New Algoriyhm for Processing Interferometric Data-Stacks: SqueeSAR. IEEE Trans., Geosci., Remote Sensing, Vol. 38, N0. 5, P. 3460-3470.
6. Fekir, M., Hocine, F., Belhadj-aissa, M., Haddoud, A., et Belhadj-aissa, A. (2013). Coherent Targets Selection based on Small Baseline interferogram Subsets", IEEE, 978-1-4673-6396-9/13.
7. Berardino, P., Fornaro, G., Lanari, R. et Sansosti, E. (2002). A New Algorithm for Surface Deformation Monitoring Based on Small Baseline Differential SAR Interferograms. IEEE Transactions on Geoscience and Remote Sensing, Vol. 40, N0.11, p. 2375–2383.
8. Mora, O., Mallorqui, J. J., & Broquetas, (2003). A linear and nonlinear terrain deformation maps from a reduced set of interferometric SAR images". Geoscience and Remote Sensing, IEEE Transactions on, Vol. 41, N0.10, p. 2243–2253,
9. Lanari, R., Mora, O., Manunta, M., Mallorqui, J. J., Berardino, P., et Sansosti, E. (2004). A small-baseline approach for investigating deformations on full-resolution differential SAR interferograms. IEEE Transactions on Geoscience and Remote Sensing, 42, p. 1377–1386